

pubs.acs.org/cm Article

Synthesis and Structural Anisotropy of Single-Crystalline 2D AgEPh (E = S, Se, Te)

Woo Seok Lee, Peter Müller, Nicholas Samulewicz, Tejas Deshpande, Ruomeng Wan, and William A. Tisdale*



Cite This: Chem. Mater. 2024, 36, 9904-9913



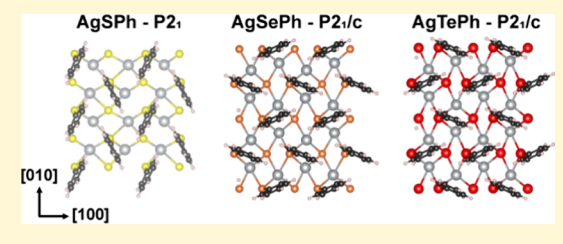
ACCESS I

III Metrics & More

Article Recommendations

sı Supporting Information

ABSTRACT: Silver phenylchalcogenides (AgEPh; E = S, Se, Te) are emerging two-dimensional (2D) semiconductors belonging to a broader class of hybrid organic—inorganic materials, known as metal organochalcogenolates (MOCs). However, it has been challenging to synthesize crystals of AgSPh and AgTePh that are sufficient for fundamental and applied research. Moreover, assignment of the crystal structure of AgSePh is debated (C2/c vs $P2_1/c$). Here, we report the growth of up to millimeter-sized single-crystalline 2D AgEPh (E = S, Se, or Te) having a macroscopic parallelogram shape.



Transmission electron microscopy and electron diffraction studies reveal the relationship between their macroscopic morphology and microscopic crystal structure, which is essential for understanding in-plane anisotropic properties. We report three new crystal structures through single-crystal X-ray diffraction: 2D AgSPh in P2₁ and 2D AgTePh in $P2_1/c$, as well as 1D AgTeC_{6.27}H_{5.62}N_{0.09} (1D AgTePh + 0.089C₃H₇N) in P1̄. Significantly, our space group assignment of all three 2D AgEPh compounds in primitive lattices is different from that of the previously reported C-centered lattices. Using temperature-dependent powder X-ray diffraction and temperature-dependent absorption and photoluminescence spectroscopy of 2D AgEPh prepared by different synthetic methods, we reconcile discrepancies in their structural assignment, which is needed for the accurate theoretical prediction of electronic and vibrational properties.

■ INTRODUCTION

Metal organochalcogenolates (MOCs) are an emerging class of low-dimensional hybrid organic—inorganic semiconductors with a chemical formula of [M(ER)],, where M typically stands for coinage metals [Cu(I), Ag(I), and Au(I)]; E for chalcogen elements (S, Se, Te); and R for an organic hydrocarbon. ^{1–3} Unlike other low-dimensional hybrid materials such as colloidal nanocrystals or halide perovskites, MOCs are distinguished by the covalent bonds between their inorganic and organic components. This covalent bonding enables structural, dimensional, and electronic tunability through both organic functionalization and inorganic component manipulations. ^{3,8,14–21} Consequently, MOCs find applications across a broad range of fields, including catalysis, ^{17,20} sensing, ^{10,22–25} light emission, ^{11,15,21,26} and electronic devices. ^{27,28}

Silver phenylthiolate (AgSPh, also known as "thiorene"), $^{17-20}$ silver phenylselenolate (AgSePh, also known as "mithrene"), $^{17,18,20,26,29-31}$ and silver phenyltellurolate (AgTePh, also known as "tethrene") $^{17-19,21}$ are prototypical examples of two-dimensional (2D) MOCs. These compounds form layered van der Waals solids, where inorganic silver chalcogenide layers are sandwiched between benzene rings extending above and below the inorganic plane. Among these, AgSePh has received the most attention due to its narrow blue (~467 nm) emission, $^{8,18,19,21,23,24,26,29-35}$ while AgSPh ex-

hibits no photoluminescence 18,19 and AgTePh shows a broad emission centered at ~600 nm with a significant Stokes shift. 18,19,21 Initially, the crystal structures of these compounds were refined to monoclinic C-centered lattices (AgSPh in Cc, 18 AgSePh, 18,31 and AgTePh in C2/c). Recently, our team developed an amine-assisted reaction method, enabling the growth of millimeter-sized single-crystalline AgSePh whose structure was refined to the P2₁/c space group.³⁰ However, whether this amine-assisted method could be extended to grow large, high-quality crystals of other chalcogen analogues has remained unproven. More significantly, despite the importance of the crystal structure for accurate theoretical calculations and further material property optimization, assignment of the crystal structure of AgSePh $(C2/c \text{ vs } P2_1/c)$ remained a subject of debate. 18,30,31 Finally, knowledge of the relationship between the microscopic crystal structure and the macroscopic growth habit of these crystals is essential for the characterization of their anisotropic properties.

Received: July 26, 2024

Revised: September 23, 2024 Accepted: September 25, 2024 Published: September 30, 2024





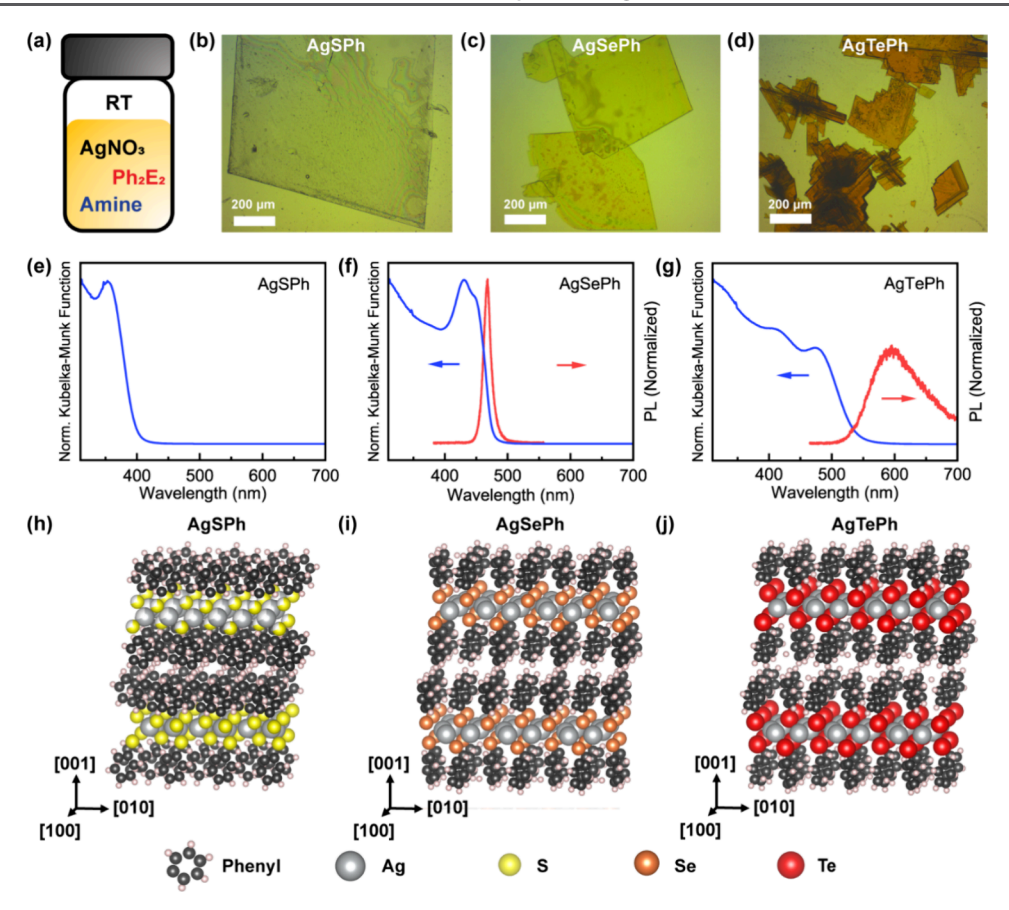


Figure 1. Structural and optical properties of AgEPh (E = S, Se, Te) crystals synthesized by (a) the amine-assisted solution phase reaction method. Optical micrographs of (b) AgSPh, (c) AgSePh, and (d) AgTePh crystals. Diffuse reflectance UV—vis absorption and photoluminescence spectra of (e) AgSPh, (f) AgSePh, and (g) AgTePh crystals. Crystal structures of (h) AgSPh (monoclinic $P2_1$), (i) AgSePh (monoclinic $P2_1/c$), and (j) AgTePh (monoclinic $P2_1/c$) determined by single-crystal X-ray diffraction. Disordered atoms in AgSPh have been omitted for clarity.

Here, we report the growth of up to millimeter-sized singlecrystalline AgEPh (E = S, Se, or Te) with a unique macroscopic parallelogram shape. Through transmission electron microscopy and electron diffraction studies, we reveal the relationship between the macroscopic morphology of 2D AgEPh and the microscopic crystal structure. Furthermore, we determine three new crystal structures through single-crystal Xray diffraction: 2D AgSPh in P2₁ and 2D AgTePh in $P2_1/c$ as well as 1D AgTeC_{6.27} $H_{5.62}N_{0.09}$ (1D AgTePh + 0.089 C_3H_7N) in P1. We explore and discuss potential causes for the discrepancies in crystal structure descriptions of 2D AgEPh (primitive lattices in this work vs C-centered lattices in previous works), such as phase transitions, polymorphism, and differences in crystal quality and diffraction data collection methods, and we present temperature-dependent powder Xray diffraction and temperature-dependent absorption and photoluminescence spectroscopy of 2D AgEPh prepared from different synthetic methods to support our conclusions.

RESULTS AND DISCUSSION

Synthesis, Structural, and Optical Characterization of AgEPh (E = S, Se, Te). 2D AgEPh (E = S, Se, Te) crystals were synthesized by the amine-assisted solution phase method with a slight modification (Figure 1a). Briefly, a 20 mM solution of silver nitrate (AgNO₃) in 1-butylamine (BuNH₂) and a 20 mM solution of diphenyl dichalcogenide (Ph₂E₂; E = S, Se, or Te) in BuNH₂ were mixed in a sealed vial. The vial was then stored under dark at room temperature for 2 weeks to

obtain AgSPh crystals, 3 days for AgSePh crystals, and 2 months for AgTePh crystals. The lateral sizes of the AgEPh crystals vary from $\sim 10 \ \mu m$ to even larger than $\sim 1 \ mm$ (Figure 1b-d and Figure S1), with thicknesses ranging from submicron to tens of microns. For AgSPh and AgSePh, no byproduct or intermediate phase was observed during the synthesis process, and similar results were obtained when propylamine (PrNH₂) and hexylamine (HexNH₂) were used instead of BuNH2. However, for AgTePh, 1D fibers initially emerged within a few hours after the precursors were mixed in BuNH₂. After 1 week to a month, 2D AgTePh crystals began to appear and grow, accompanied by a loss of 1D fibers, implying a chemical transformation of 1D fibers to 2D AgTePh. After 2-3 months, only 2D AgTePh crystals were observed. Similar results were observed when PrNH2 and HexNH₂ were used instead of BuNH₂. All three 2D AgEPh crystals were too large to form a stable colloidal solution.

In one experiment, mixing a solution of $AgNO_3$ in $PrNH_2$ with a solution of Ph_2Te_2 in toluene resulted in the formation of 1D crystals after 1 week with no appearance of 1D fibers and 2D AgTePh throughout the entire synthesis period. The crystal structure of 1D crystals was determined through single-crystal X-ray diffraction (SCXRD), revealing a triclinic $P\overline{1}$ space group with a chemical formula of $AgTeC_{6.27}H_{5.62}N_{0.09}$ (1D $AgTePh+0.089\ C_3H_7N$), where the amine solvent was trapped within a channel between chains of 1D AgTePh (Figure S2 and Table 1). Notably, powder X-ray diffraction patterns and photoluminescence spectra of 1D fibers (with unknown crystal

Table 1. Crystal Data and Structure Refinement of 2D AgSPh, 2D AgTePh, and 1D AgTe $C_{6.27}H_{5.62}N_{0.09}$ (1D AgTePh + $0.089C_3H_7N$)

	2D AgSPh	2D AgTePh	$1D AgTePh + 0.089C_3H_7N$
identification code	P23051	P23058	P21094
empirical formula	C_6H_5AgS	C_6H_5AgTe	$C_{6.27}H_{5.62}AgN_{0.09}Te$
formula weight	217.03	312.57	317.64
temperature	100(2) K	100(2) K	100(2) K
wavelength	0.71073 Å	0.71073 Å	0.71073 Å
crystal system	monoclinic	monoclinic	triclinic
space group	P2 ₁	P2 ₁ /c	$P\overline{1}$
unit cell dimensions	$a = 7.3481(10) \text{ Å}, \ \alpha = 90^{\circ}$	$a = 5.8218(2) \text{ Å}, \ \alpha = 90^{\circ}$	$a = 4.81028(10)$ Å, $\alpha = 79.9448(10)$
	$b = 5.8045(7) \text{ Å}, \beta = 94.111(4)^{\circ}$	$b = 7.4781(3) \text{ Å}, \beta = 92.9041(15)^{\circ}$	$b = 12.8426(3) \text{ Å}, \beta = 84.5318(9)^{\circ}$
	$c = 28.134(4) \text{ Å}, \gamma = 90^{\circ}$	$c = 30.1349(13) \text{ Å}, \gamma = 90^{\circ}$	$c = 17.2883(4) \text{ Å}, \gamma = 83.1369(9)^{\circ}$
volume	1196.9(3) Å ³	1310.27(9) Å ³	$1041.04(4) \text{ Å}^3$
Z	8	8	6
density (calculated)	2.409 Mg/m^3	3.169 Mg/m^3	3.040 Mg/m^3
absorption coefficient	3.585 mm ⁻¹	7.322 mm ⁻¹	6.915 mm ⁻¹
F(000)	832	1120	857
crystal size	$0.415 \times 0.355 \times 0.035 \text{ mm}^3$	$0.235 \times 0.070 \times 0.010 \text{ mm}^3$	$0.200 \times 0.015 \times 0.005 \text{ mm}^3$
theta range for data collection	1.451 to 31.587°.	2.707 to 31.551°	1.619 to 31.583°
index ranges	$-10 \le h \le 10$	$-8 \le h \le 8$	$-7 \le h \le 6$
	$-8 \le k \le 8$	$-10 \le k \le 11$	$-18 \le k \le 18$
	$-41 \le l \le 41$	$-44 \le l \le 44$	$-25 \le l \le 25$
reflections collected	61611	69667	91707
independent reflections	7992 [R(int) = 0.0518]	4361 [R(int) = 0.0389]	6924 [R(int) = 0.0434]
completeness to theta = 25.242°	99.70%	99.80%	99.90%
absorption correction	semiempirical from equivalents	semiempirical from equivalents	semiempirical from equivalents
refinement method	full-matrix least-squares on F^2	full-matrix least-squares on F^2	full-matrix least-squares on F^2
data/restraints/parameters	7992/669/328	4361/0/145	6924/1409/429
goodness of fit on F2	1.117	1.03	1.1
final R indices $[I > 2 \operatorname{sigma}(I)]$	R1 = 0.0879, wR2 = 0.2489	R1 = 0.0252, wR2 = 0.0581	R1 = 0.0203, $wR2 = 0.0325$
R indices (all data)	R1 = 0.0978, $wR2 = 0.2591$	R1 = 0.0370, wR2 = 0.0655	R1 = 0.0279, $wR2 = 0.0349$
absolute structure parameter	0.43(14)	n/a	n/a
extinction coefficient	0.0060(13)	n/a	n/a
largest diff. peak and hole	6.749 and -8.434 e.Å ⁻³	1.345 and −1.217 e.Å ⁻³	1.045 and -0.947 e.Å ⁻³

structure and composition), 1D AgTeC $_{6.27}$ H $_{5.62}$ N $_{0.09}$ crystals, and 2D AgTePh crystals are all different, suggesting they are all different materials (Figure S2). Therefore, careful attention and the choice of solvent were needed to obtain 2D AgTePh crystals.

Diffuse reflectance UV-vis absorption and photoluminescence (PL) spectra of AgEPh crystals at room temperature are shown in Figure 1e-g. The AgSPh crystals exhibited an absorption peak centered around 355 nm (~3.49 eV), but no detectable PL was observed when they were excited by 355 nm light. The AgSePh crystals exhibited two overlapping absorption features at 431 and 452 nm (~2.87 and ~2.74 eV). Upon excitation with 405 nm light, the AgSePh crystals displayed PL centered at 467 nm (~2.65 eV) with a full width at half-maximum (FWHM) of ~76 meV, previously assigned to band-edge exciton emission.²¹ The AgTePh crystals revealed two identifiable absorption peaks with large energetic separation, centered at 417 and 477 nm (~2.97 and ~2.59 eV). When excited by 405 nm light, the AgTePh crystals exhibited a significantly red-shifted and broadened PL peak centered at 597 nm (~2.07 eV) with an FWHM of ~382 meV, previously assigned to self-trapped exciton emission.²¹

The AgEPh crystals exhibit excellent crystallinity sufficient for SCXRD. In our previous work, we reported the crystal structure of AgSePh in the monoclinic $P2_1/c$ space group determined through SCXRD at 100 K (Figure 1i).³⁰ In this

work, we additionally report new crystal structures for AgSPh in the monoclinic $P2_1$ space group and AgTePh in the monoclinic $P2_1/c$ space group determined through SCXRD at 100 K. All three compounds AgSePh, AgSPh, and AgTePh exist as 2D layered structures consisting of inorganic AgE layers with in-plane anisotropy, which are sandwiched between layers of benzene rings that are covalently bound to each chalcogen atom (see Supplementary Note, Figure 1h—j, and Table 1). The single-crystalline nature of these materials is further revealed by using polarized light microscopy (Figure (3))

Relationship between the Macroscopic Morphology and Microscopic Structure. The AgEPh single crystals tend to exhibit a parallelogram shape, featuring acute angles of 76–78° and obtuse angles of 102–104° (Figure 1b–d and Figures S1 and S3). To explore the relationship between the macroscopic morphology and microscopic crystal structure, we performed transmission electron microscopy (TEM) and electron diffraction (ED) analysis on AgEPh single crystals (Figure 2). Diffraction spots were indexed with (*hkl*) values by comparing them to simulated ED patterns based on crystallographic information obtained *via* SCXRD (Figure S4). The crystallographic [100] and [010] axes were then presented by drawing lines from the origin toward (*h*00) and (0*k*0) diffraction spots, respectively (see Supplementary Note and Figure S5). By superimposing these crystallographic axes onto

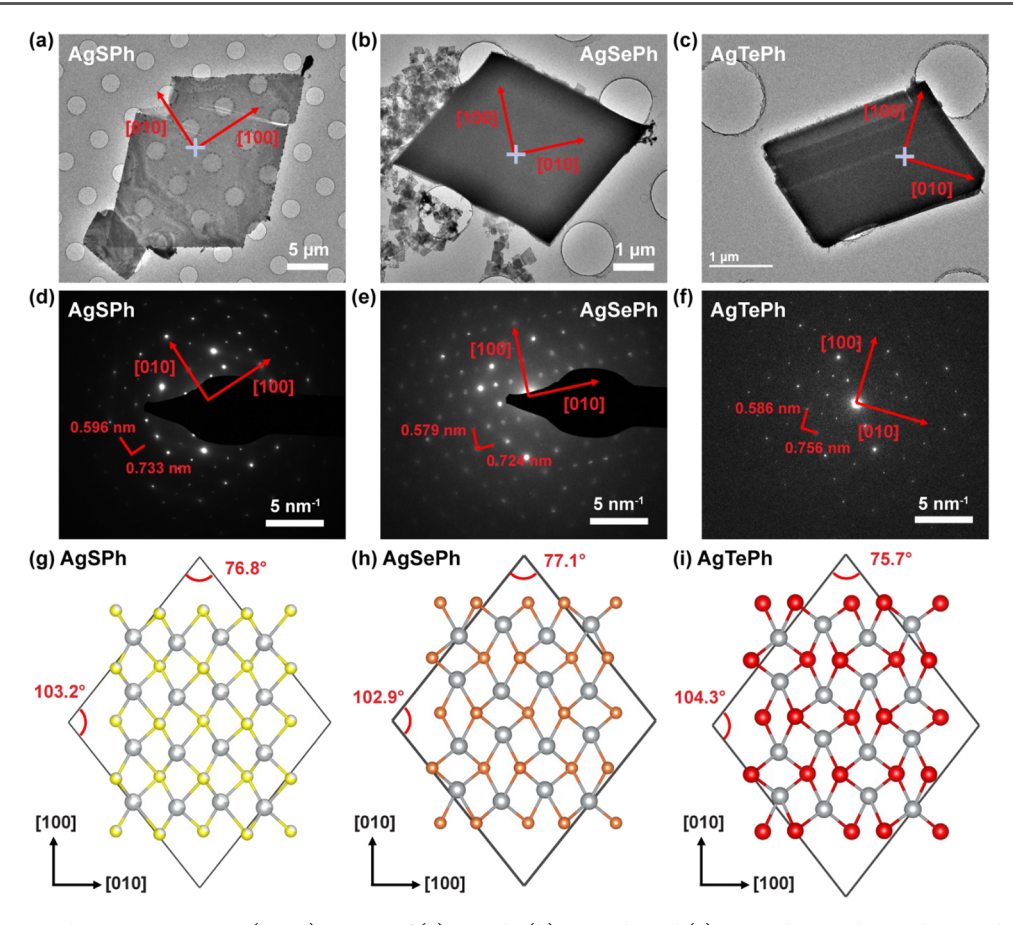


Figure 2. Transmission electron microscopy (TEM) images of (a) AgSPh, (b) AgSePh, and (c) AgTePh crystals. Single-crystal electron diffraction (ED) patterns of (d) AgSPh, (e) AgSePh, and (f) AgTePh at marked locations in (a–c). The red arrows indicate the in-plane crystallographic axes determined through a comparison between experimental ED patterns (d–f) and simulated ED patterns (Figure S4) based on crystallographic information. The real-space distance corresponding to each pair of diffraction peaks is also annotated. Crystal structures of (g) AgSPh in $P2_1/c$, (h) AgSePh in $P2_1/c$, and (i) AgTePh in $P2_1/c$, depicted along the crystallographic [001] orientation. Phenyl rings are omitted for clarity. The parallelograms outlined with a black solid line depict expected growth habit of macroscopic crystals terminated by {110} planes.

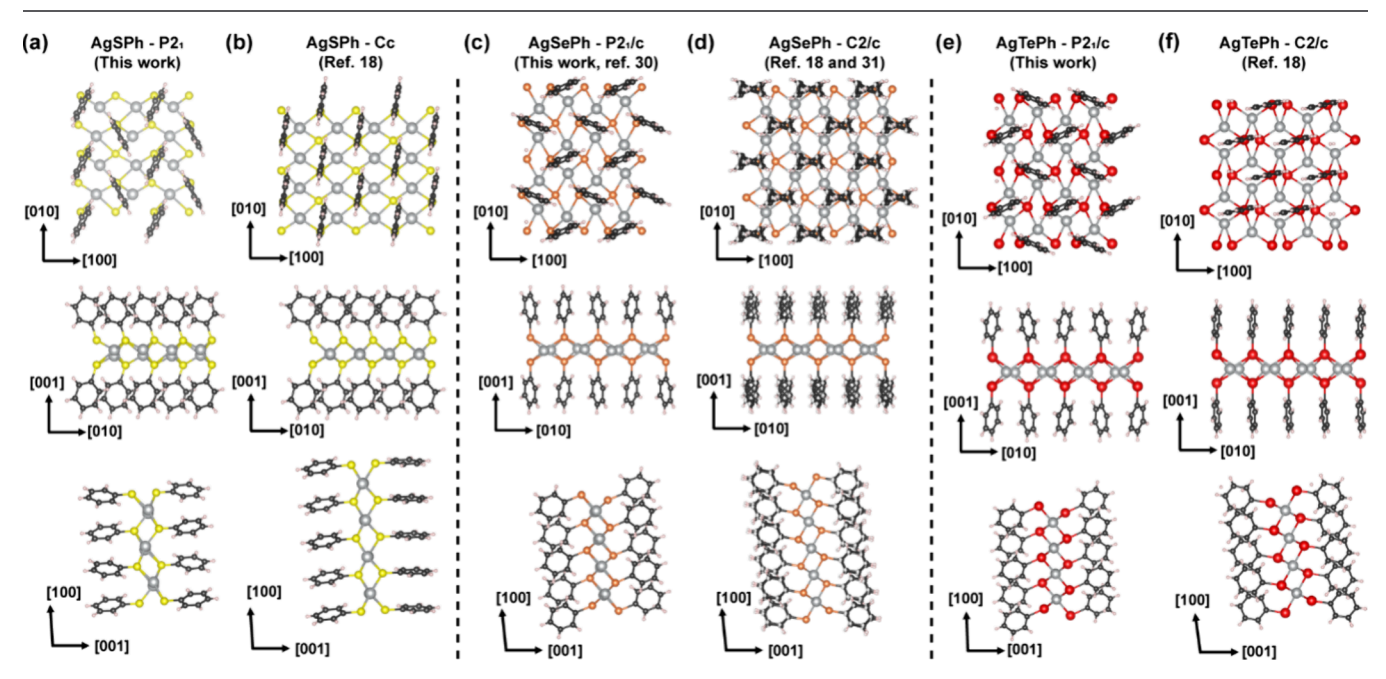


Figure 3. Crystal structures of AgSPh in (a) $P2_1$ and (b) Cc (ref 18), AgSePh in (c) $P2_1/c$ (ref 30), and (d) C2/c (refs 18 and 31), and AgTePh in (e) $P2_1/c$ and (f) C2/c (ref 18), depicted along crystallographic [001] (top), [100] (middle), and [010] (bottom) directions. In the [001] view, benzene rings at the bottom of the AgE plane are omitted for clarity. Disordered atoms in AgSPh in $P2_1$ are omitted for clarity.

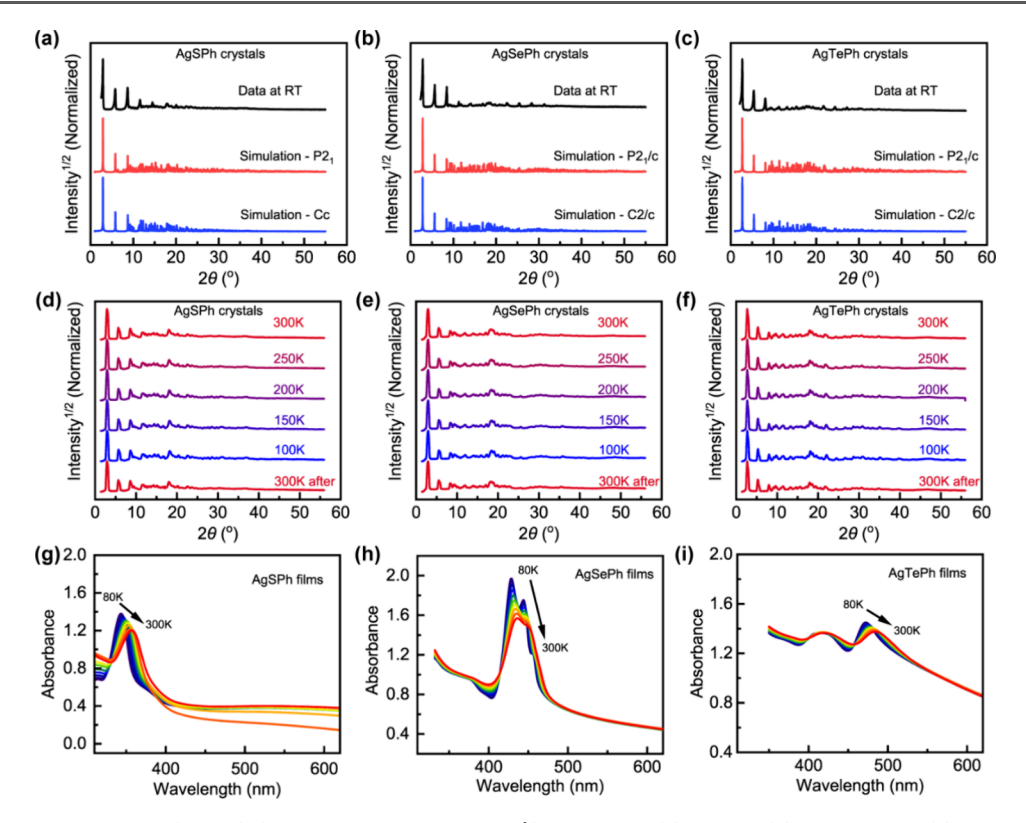


Figure 4. Powder X-ray diffraction (PXRD) (Mo $K\alpha$ radiation, λ = 0.71 Å) patterns of (a) AgSPh, (b) AgSePh, and (c) AgTePh crystals and the corresponding simulated patterns based on crystallographic information of primitive structures (red, this work and ref 30) and C-centered structures (ref 18). Temperature-dependent PXRD patterns of (d) AgSPh, (e) AgSePh, and (f) AgTePh crystals. Temperature-dependent absorption spectra of (g) AgSPh, (h) AgSePh, and (i) AgTePh films obtained by the tarnishing method.

the TEM images corresponding to the ED patterns, we found that for AgSPh, the [100] and [010] axes align with directions toward acute and obtuse angles, respectively. Conversely, for AgSePh and AgTePh, the [010] and [100] axes align with directions toward acute and obtuse angles, respectively. Building confidence in these assignments, schematic illustrations of hypothetical crystals terminated with {110} planes closely resemble the actual macroscopic crystals in terms of their parallelogram shape, angles, and crystal orientation (Figure 2g–i). These findings establish useful correlations between experimental observations on macroscopic crystals and their underlying microscopic structure, which will aid comparison between experimental observations of optical and electrical anisotropy and theoretical calculations in future investigations.

Discrepancies in Crystal Structure Descriptions of AgEPh (E = S, Se, Te). The crystal structures we report here differ from previous reports in terms of space group assignment, organization of the silver-chalcogen network, and arrangement of the phenyl ligand array at room temperature (Figure 3). 18,30,31 For instance, whereas AgSPh in Cc exhibits nearly linear Ag-Ag chains along the [010] direction, AgSPh in P2₁ shows distorted and zigzag Ag-Ag chains (see Table S1 and Figure S6 for details on the Ag-Ag and Ag-S bond parameters of AgSPh in P2₁ and in Cc). More strikingly, whereas AgEPh in C-centered structures exhibits a linear arrangement of benzene rings (AgSPh and AgTePh) or disordered benzene rings (AgSePh), AgEPh in primitive structures exhibits a herringbone arrangement of benzene rings. Considering the organic-inorganic hybrid nature of the AgEPh electronic and vibrational band structure, 21,32 the

discrepancy in both inorganic structures and the arrangement of organic ligands between primitive structures and C-centered structures is significant for our understanding of their fundamental properties.

In a previous report of C-centered lattices, AgEPh crystallites were synthesized by the reaction between silver(I) oxide (or metallic silver) and benzeneselenol or benzenethiol (or diphenyl ditelluride) with isopropanol at 70–100 °C. ¹⁸ The structures of these compounds were then determined by using a novel serial femtosecond X-ray crystallography method performed on colloidal dispersions of crystallites at room temperature. Possible explanations for differences in crystallographic assignment (primitive vs C-centered) include (1) phase transformations occurring between 100 K and room temperature, ³⁶ (2) differences in the reaction products obtained by different synthetic methods, ³⁷ or (3) differences in crystal quality or diffraction data collection methods. ^{38,39}

To explore the possibility of a phase transition between 100 and 300 K, we conducted temperature-dependent powder X-ray (Mo K α radiation, λ = 0.71 Å) diffraction (PXRD) measurement of ground AgEPh crystals (Figure 4a–f). Peaks in the PXRD pattern monotonically shifted to smaller angles as temperature decreased due to unit cell contraction. However, the overall diffraction pattern and relative peak intensities were maintained without the disappearance of existing diffraction peaks or the emergence of new diffraction peaks, suggesting no phase transition. Given that the simulated PXRD patterns of primitive unit cells and C-center unit cells are very similar to each other (Figure 4a–c), it is also possible that our instrument's resolution and sensitivity were not sufficient to detect a potential phase transition. To further evaluate the

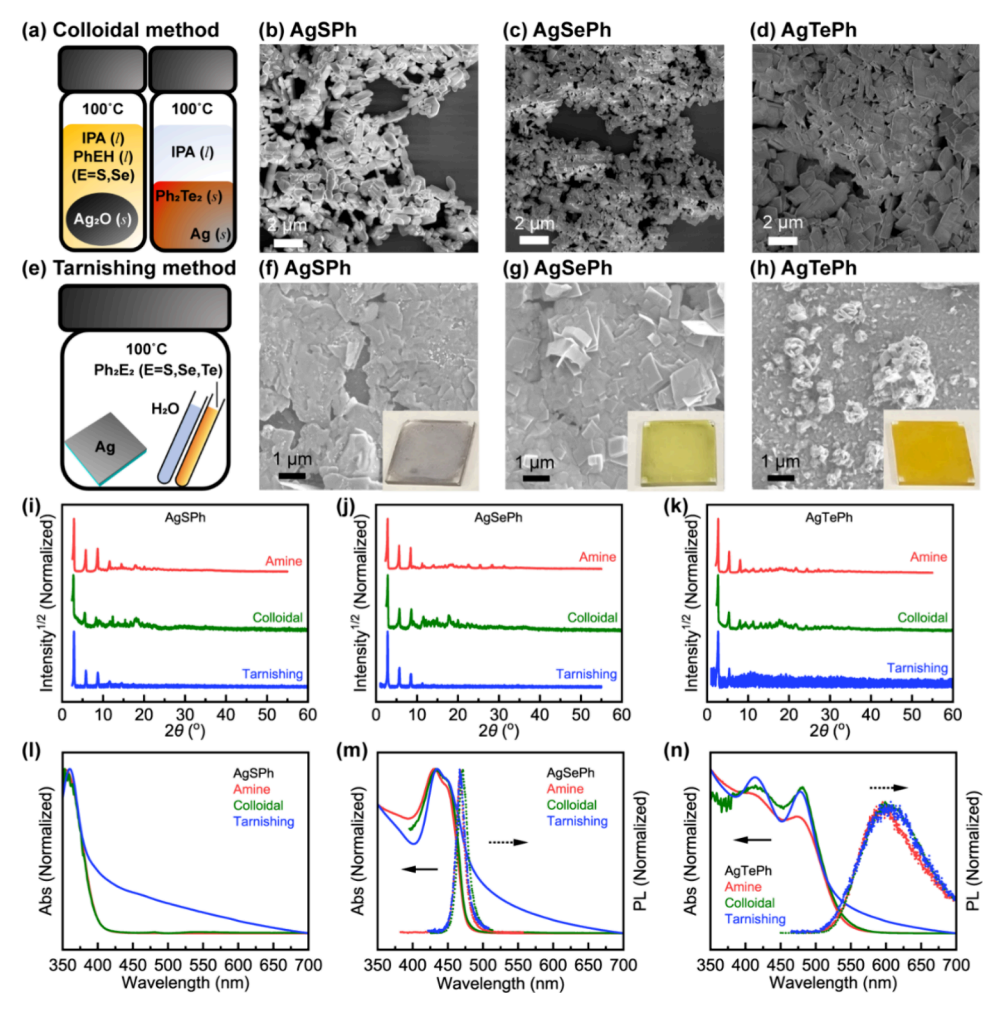


Figure 5. (a) Schematic illustration of the colloidal synthesis method, ¹⁸ and scanning electron microscopy (SEM) images of (b) AgSPh, (c) AgSePh, and (d) AgTePh nanocrystals obtained by the colloid method. (e) Schematic illustration of the tarnishing method, ²⁹ and SEM images of (f) AgSPh, (g) AgSePh, and (h) AgTePh thin films obtained by the tarnishing method. The insets show photographs of AgEPh films on a glass substrate with dimensions of 12.2 mm × 1.2 mm × 1.1 mm. Powder X-ray diffraction (PXRD) (Mo Kα radiation, λ = 0.71 Å) patterns of (i) AgSPh, (j) AgSePh, and (k) AgTePh single crystals (red), colloidal crystallites (green), and thin films (blue) obtained by the amine-assisted method, the colloidal method, and the tarnishing method, respectively. Diffuse reflectance UV—vis absorption and photoluminescence spectra of (l) AgSPh, (m) AgSePh, and (n) AgTePh crystals, obtained by the amine-assisted method, the colloidal method, and the tarnishing method, respectively.

possibility of a phase transition, we performed temperature-dependent optical absorption measurement of AgEPh films, which is typically a more sensitive indicator of phase changes in hybrid semiconductors (Figure 4g–i).^{36,40} However, no evidence of a phase transition was detected using temperature-dependent absorption; the only spectral changes observed are those expected from reduced dynamic disorder at a lower sample temperature and temperature-dependent electron—phonon coupling (note: To obtain partially transparent thin films for optical transmission studies, AgEPh films were prepared by the "tarnishing method", wherein a thin metallic silver film is reacted with vapor-transported diphenyl dichalcogenides at 100 °C in the presence of water vapor, Figure 5e–h).^{21,24,29}

Next, we compared the measured properties of AgEPh materials produced by different synthesis methods (Figure 5). This comparison included the amine-assisted method, where AgEPh was determined in primitive lattices, and the colloidal method, where AgEPh was determined in C-centered lattices, 18 as well as the tarnishing method, 29 where temper-

ature-dependent absorption measurements were performed. The synthesis conditions for 2D AgEPh by the amine-assisted method (Figure 1a), 30 the colloidal method (Figure 5a), 18 and the tarnishing method 29 (Figure 5e) are all different in terms of precursors, solvents, and reaction temperatures. To assess whether 2D AgEPh obtained from different methods is an identical material or polymorph, we compared their structural and optical properties (Figure 5i–n). (Note: for AgEPh films grown by the tarnishing method, only the (00h) diffraction peaks were observed due to a strong preference for crystal growth with the c-axis perpendicular to the substrate.) 24,29

Having concluded that neither differences in the reaction products (i.e., polymorphism) nor temperature-dependent phase transitions are likely explanations for discrepancies in crystallographic assignment, we turn our attention now to the possibility of differences in crystal quality and/or data collection methods. Structures of AgEPh were previously assigned to C-centered lattices. However, for AgSPh, we found no indication of any lattice centering in our data (Table S2). In the cases of AgSePh and AgTePh, although C-lattice

reflections are systematically weaker than the average, they were still clearly observed (Tables S3 and S4). Nevertheless, we attempted to determine the structures of AgSePh and AgTePh in C-centered lattices, and reasonable models could be established in space group C2/c for both (Figure S7). However, it should be noted that in this space group, we encountered over 10,000 systematic-absence violations, and the phenyl ring is disordered over two positions with a 50:50 ratio. Although R-values are slightly lower in the C2/c model (as expected when over 10,000 of the weakest reflections are excluded), we believe the description in space group $P2_1/c$ is superior to that in C2/c for AgSePh and AgTePh based on our data because the primitive structures make use of all collected data and, therefore, contain all information. The AgEPh crystallites obtained by the methods reported in ref 18 have lateral dimensions in the order of a few micrometers or smaller and a thickness in the submicrometer range (Figure 5b-d). For these smaller crystallites, systematically weak X-ray reflections may not rise above the signal-to-noise ratio of the detector. ^{38,39} In contrast, the size of AgSPh, AgSePh, ³⁰ and AgTePh crystals used for SCXRD reported here were 415 μm \times 355 μ m \times 35 μ m, 230 μ m \times 220 μ m \times 20 μ m, and 235 μ m \times 70 μ m \times 10 μ m, respectively (Figure S8 and ref 30). Additionally, the suppression of defect-derived PL in AgSePh crystals obtained by the amine-assisted method, as previously reported, further supports high crystal quality.³

Finally, it is possible that the serial femtosecond X-ray crystallography method used in ref 18 might make it more difficult to record systematically weak reflections, as those authors mentioned in their conclusion that access to higher beam energies in the future will further improve the resolution of this emerging technique. Indeed, recent X-ray free-electron laser work with high-energy photons providing 0.8 Å resolution supports this assertion [Paley, Hohman, private communication]. Taken together, these results reveal the need for high-resolution diffraction data in serial experiments as well as the importance of complementary methods for structural analysis.

CONCLUSIONS

In conclusion, we have demonstrated the growth of up to millimeter-sized single-crystalline AgEPh (E = S, Se, Te) and revealed the relationship between their macroscopic morphology and microscopic crystal structures. We report three new structures (2D AgSPh, 2D AgTePh, and 1D AgTePh + 0.089C₃H₇N), and we addressed discrepancies in the crystallographic assignment of 2D AgEPh (primitive lattices vs Ccentered lattices). We concluded that 2D AgEPh materials grown by the amine method,³⁰ the colloidal method,¹⁸ or the tarnishing method²⁹ all adopt the same phase and that these structures are best described by a primitive lattice. Considering the growing interest in these emerging 2D hybrid materials, this work paves the way for future experimental and theoretical investigations into in-plane anisotropic electronic, optical, and vibrational properties arising from their low-symmetry structures.

EXPERIMENTAL METHODS

Chemicals. Silver pellets (Ag, 99.99% pure) were purchased from Kurt J. Lesker. Diphenyl disulfide (Ph_2S_2 , 99.0+%), diphenyl diselenide (Ph_2Se_2 , 97.0+%), and benzeneselenol (PhSeH, >95.0%) were purchased from TCI America. Diphenyl ditelluride (Ph_2Te_2 , 98%), benzenethiol (\geq 99%), propylamine ($PrNH_2$, 98%), butylamine

(BuNH₂, 99.5%), hexylamine (HexNH₂, 99%), toluene (>99.5%), isopropanol (IPA, \geq 99.5%), potassium bromide (KBr, 99.0%) silver powders (Ag, \geq 99.9%), silver nitrate (AgNO₃, \geq 99.0%), and silver(I) oxide (Ag₂O₃, \geq 99.99%) were purchased from Millipore Sigma.

Preparation of AgEPh (E = S, Se, Te) Crystals by the Amine-Assisted Method.³⁰ AgEPh crystals were synthesized by mixing a 20 mM solution of silver nitrate (AgNO₃) in 1-butylamine (BuNH₂) and a 20 mM solution of diphenyl dichalcogenide (Ph₂E₂) in BuNH₂ in a sealed vial (Figure 1a). The vial was then stored under dark at room temperature for 2 weeks to obtain AgSPh crystals, 3 days for AgSePh crystals, and 2 months for AgTePh crystals. For AgSPh and AgSePh, no byproduct or intermediate phase was observed during the synthesis process, and similar results were obtained when propylamine (PrNH₂) and hexylamine (HexNH₂) were used instead of BuNH₂. However, for AgTePh, 1D fibers with an unknown structure and composition initially emerged within a few hours after mixing precursors in BuNH₂. After 1 week to a month, 2D AgTePh crystals began to appear and grow, accompanied by a loss of 1D fibers, implying a chemical transformation of 1D fibers to 2D AgTePh. After 2-3 months, only 2D AgTePh crystals were observed. Similar results were observed when PrNH2 and HexNH2 were used instead of BuNH₂. In one experiment, mixing a solution of AgNO₃ in PrNH₂ with a solution of Ph2Te2 in toluene resulted in the formation of 1D $AgTeC_{6.27}H_{5.62}N_{0.09} \ crystals \ (1D \ AgTePh \ + \ 0.089C_3H_7N) \ after \ 1$ week, with no appearance of 1D fibers and 2D AgTePh throughout the entire synthesis period. Therefore, careful attention and choice of solvent were needed to obtain 2D AgTePh crystals.

Preparation of Colloidal AgEPh (E = S, Se, Te) Crystallites. ¹⁸
For AgSPh and AgSePh nanocrystals, 100 mg of silver(I) oxide was placed in a 5 mL glass vial with 1 mL of isopropyl alcohol and 1 mL of benzenethiol (PhSH) or benzeneselenol (PhSeH). The vial was sealed and placed in a secondary container to avoid leakage of toxic and smelly PhSH or PhSeH. The vial was heated in an oven at 100 °C for 1 day to obtain AgSPh or AgSePh crystals. For AgTePh crystals, 100 mg of metallic silver powders and 1.5 g of diphenyl ditelluride (Ph₂Te₂) were placed in a 5 mL glass vial with 1 mL of IPA. The vial was sealed and placed in a secondary container. The container was heated in an oven at 100 °C for 4 days to obtain AgTePh crystals. AgEPh crystals were retrieved after removing excess organic ligands by three cycles of centrifugation (6000 rpm for 2 min) with toluene, IPA, and ethanol, successively.

Preparation of AgEPh (E = S, Se, Te) Thin Films by the Tarnishing Method. AgEPh thin films were prepared by a chemical transformation reaction between metallic silver and a vapor of Ph₂E₂, known as the tarnishing method. Silver films with thickness of 15 nm were deposited on precleaned glass substrates (12.2 × 12.2 × 1.1 mm³, Luminescence Technology Corp.) by thermal evaporation with a deposition rate of ~1 Å/s. After that, the prepared silver films, Ph₂E₂ powder, and 200 μ L of deionized water in separate open culture tubes were sealed together inside a microwave reaction vial. After heating in an oven at 100 °C for 4–7 days, the silver films transformed into AgEPh films.

Sample Storage. 2D AgEPh crystals grown by amine, colloidal, and tarnishing methods are all stable under ambient air conditions, but they are all similarly unstable under high laser power or prolonged light exposure. Therefore, all materials were stored in a drawer and protected from light, except during spectroscopic measurements.

Polarized Optical Microscopy. Samples supported on transparent glass coverslips were mounted in an inverted microscope (Nikon Ti–U Eclipse). Above and below the sample, a polarizer and an analyzer were placed orthogonally to each other. The sample was illuminated by an overhead broadband white light source (Nikon D-LH Halogen 12 V 100W). The transmitted light through the sample was collected with an objective lens (Nikon, CFI S Plan Fluor ELWD, 40×, 0.6 NA) and then directed into a color CMOS camera (Thorlabs, DCC1645C-HQ). Polarized optical images were taken by rotating the sample stage.

Photoluminescence Spectroscopy. PL spectra of AgSePh and AgTePh were measured with a home-built setup consisting of an inverted microscope (Nikon, Ti–U Eclipse) equipped with a 405 nm

laser diode (PicoQuant, LDHDC-405M, continuous-wave mode) and a cooled charge-coupled detector (Princeton Instruments, PiMAX 4) on a spectrograph (Princeton Instruments, SP-2500). A Tecan Spark multimode plate reader with 355 nm excitation was used to measure the PL of AgSPh, but no PL was detected (AgSePh and AgTePh showed measurable signal under the same conditions).

UV-Vis Spectroscopy and Diffuse Reflectance Spectroscopy. Absorption spectra of AgEPh films prepared by the tarnishing method were obtained by using a Cary 5000 UV-vis-NIR spectrometer. For temperature-dependent absorption spectra, samples were mounted inside a steady-flow Janis ST-100 optical cryostat. The cryostat was then mounted in the Cary spectrometer, evacuated to below 3×10^{-5} Torr, and cooled with liquid nitrogen. The temperature was controlled with a model 335 Lakeshore temperature controller. Diffuse reflectance spectra of AgEPh crystals prepared by the amine-assisted method and AgEPh crystallites prepared by the colloidal method were obtained using a Cary 5000 UV-vis-NIR spectrometer equipped with a PIKE Technologies DiffuseIR accessory and a PerkinElmer 1050 UV-vis-NIR spectrophotometer equipped with a diffuse reflection accessory, respectively. For diffuse reflectance measurements, AgEPh crystals and colloidal crystallites were ground with dry potassium bromide (KBr) to a ~0.3 wt % dilution and diffuse reflectance spectra were normalized to a 100% KBr baseline. The obtained diffuse reflectance spectra were converted into absorption spectra by Kubelka-Munk transform:4

$$F(R) = \frac{(1-R)^2}{2R}$$

where F(R) is the Kubelka–Munk function with a value proportional to the sample's absorption coefficient, and R is the relative reflectance of the sample with the 100% KBr baseline.

Scanning Electron Microscopy (SEM). SEM images were collected by using a Zeiss Merlin instrument operating at 1 kV and 100 pA.

Transmission Electron Microscopy (TEM) and Electron Diffraction (ED). TEM and ED were conducted by using a FEI Tecnai G2 Spirit Twin instrument operating at 120 kV.

Room-Temperature Powder X-ray Diffraction (PXRD). Room temperature PXRD data were collected using a PANalytical Empyrean X-ray diffractometer (Mo K α radiation, λ = 0.71 Å) equipped with a GaliPIX 3D detector.

Single-Crystal X-ray Diffraction (SCXRD). SCXRD data at 100 K were collected on Bruker-AXS X8 Kappa Duo diffractometers with $I\mu S$ microsources using Mo K_{α} radiation (λ = 0.71073 Å), coupled to a Photon 3 CPAD detector, performing φ and ω scans. All structures were solved by dual-space methods using SHELXT⁴² and refined against F^2 on all data by full-matrix least squares with SHELXL-2017⁴³ following established refinement strategies. All non-hydrogen atoms were refined anisotropically. All hydrogen atoms were included in the model at geometrically calculated positions and refined using a riding model. The isotropic displacement parameters of all hydrogen atoms were fixed to 1.2 times the U-value of the atoms they are linked to. Details of the data quality and a summary of the residual values of the refinements are given in Table 1. Additional crystallographic information—bond lengths and angles—can be found in the Supporting Information (Tables S5–S7).

Temperature-Dependent PXRD. Temperature-dependent transmission-mode PXRD data were collected by using the SCXRD setup.

ASSOCIATED CONTENT

Supporting Information

The Supporting Information is available free of charge at https://pubs.acs.org/doi/10.1021/acs.chemmater.4c02096.

Supplementary notes, additional figures, and crystallographic information (PDF)

Single-crystal X-ray crystallographic information on 2D AgSPh in P2₁ (CIF)

2D AgTePh in $P2_1/c$ (CIF)

Accession Codes

CCDC 2370334, 2370335, and 2370336 contain the supplementary crystallographic data for this paper. These data can be obtained free of charge via www.ccdc.cam.ac.uk/data_request/cif, or by emailing data_request@ccdc.cam.ac.uk, or by contacting The Cambridge Crystallographic Data Centre, 12 Union Road, Cambridge CB2 1EZ, UK; fax: + 44 1223 336033

AUTHOR INFORMATION

Corresponding Author

William A. Tisdale — Department of Chemical Engineering, Massachusetts Institute of Technology, Cambridge, Massachusetts 02139, United States; oorcid.org/0000-0002-6615-5342; Email: tisdale@mit.edu

Authors

Woo Seok Lee – Department of Chemical Engineering and Department of Materials Science and Engineering, Massachusetts Institute of Technology, Cambridge, Massachusetts 02139, United States; ○ orcid.org/0000-0001-9188-5104

Peter Müller – Department of Chemistry, Massachusetts Institute of Technology, Cambridge, Massachusetts 02139, United States; orcid.org/0000-0001-6530-3852

Nicholas Samulewicz – Department of Chemical Engineering, Massachusetts Institute of Technology, Cambridge, Massachusetts 02139, United States

Tejas Deshpande – Department of Chemical Engineering, Massachusetts Institute of Technology, Cambridge, Massachusetts 02139, United States

Complete contact information is available at: https://pubs.acs.org/10.1021/acs.chemmater.4c02096

Notes

The authors declare no competing financial interest.

■ ACKNOWLEDGMENTS

The authors thank Daniel W. Paley and J. Nathan Hohman for friendly conversations regarding the synthesis and structural assignment of AgEPh colloidal crystals using serial femtosecond X-ray diffraction. This work was supported by the U.S. Army Research Office under Award Number W911NF-23-1-0229. This work made use of the MRSEC Shared Experimental Facilities at MIT, supported by the National Science Foundation under award number DMR-1419807. This work was carried out in part through the use of MIT.nano's facilities. W.S.L. was partially supported by the Seoul Broadcasting System Foundation Overseas Doctoral Program Scholarship.

REFERENCES

- (1) Veselska, O.; Demessence, A. D10 Coinage Metal Organic Chalcogenolates: From Oligomers to Coordination Polymers. *Coord. Chem. Rev.* **2018**, 355, 240–270.
- (2) Wang, G.; Luo, S.; Di, T.; Fu, Z.; Xu, G. Layered Organic Metal Chalcogenides (OMCs): From Bulk to Two-Dimensional Materials. *Angew. Chem., Int. Ed.* **2022**, *61* (27), No. e202203151.

- (3) Yan, H.; Hohman, J. N.; Li, F. H.; Jia, C.; Solis-Ibarra, D.; Wu, B.; Dahl, J. E. P.; Carlson, R. M. K.; Tkachenko, B. A.; Fokin, A. A.; et al. A. Hybrid Metal—Organic Chalcogenide Nanowires with Electrically Conductive Inorganic Core through Diamondoid-Directed Assembly. *Nat. Mater.* 2017, 16 (3), 349–355.
- (4) Boles, M. A.; Ling, D.; Hyeon, T.; Talapin, D. V. The Surface Science of Nanocrystals. *Nat. Mater.* **2016**, *15* (2), 141–153.
- (5) Dey, A.; Ye, J.; De, A.; Debroye, E.; Ha, S. K.; Bladt, E.; Kshirsagar, A. S.; Wang, Z.; Yin, J.; Wang, Y.; et al. State of the Art and Prospects for Halide Perovskite Nanocrystals. *ACS Nano* **2021**, *15* (7), 10775–10981.
- (6) Kotei, P. A.; Paley, D. W.; Oklejas, V.; Mittan-Moreau, D. W.; Schriber, E. A.; Aleksich, M.; Willson, M. C.; Inoue, I.; Owada, S.; Tono, K.; Sugahara, M.; et al. Engineering Supramolecular Hybrid Architectures with Directional Organofluorine Bonds. *Small Science* **2024**, *4* (1), No. 2300110.
- (7) Aleksich, M.; Paley, D. W.; Schriber, E. A.; Linthicum, W.; Oklejas, V.; Mittan-Moreau, D. W.; Kelly, R. P.; Kotei, P. A.; Ghodsi, A.; Sierra, R. G.; et al. *J. Am. Chem. Soc.* **2023**, *145* (31), 17042–17055
- (8) Hernandez Oendra, A. C.; Aspect, M. A.; Jaeggi, J. L.; Baumann, J.; Lightner, C. R.; Pun, A. B.; Norris, D. J. Tunable Synthesis of Metal—Organic Chalcogenide Semiconductor Nanocrystals. *Chem. Mater.* **2023**, 35 (21), 9390—9398.
- (9) Yang, H.; Mandal, S.; Lee, Y. H.; Park, J. Y.; Zhao, H.; Yuan, C.; Huang, L.; Chen, M.; Dou, L. Dimensionality Engineering of Lead Organic Chalcogenide Semiconductors. *J. Am. Chem. Soc.* **2023**, *145* (44), 23963–23971.
- (10) Khamlue, R.; Sakurada, T.; Cho, Y.; Lee, W. S.; Leangtanom, P.; Taylor, M. G.; Naewthong, W.; Sripetch, P.; Na Ranong, B.; Autila, T.; et al. Heterocyclic Modification Leading to Luminescent 0D Metal Organochalcogenide with Stable X-Ray Scintillating Properties. *Chem. Mater.* **2024**, *36* (10), 5238–5240.
- (11) Hawila, S.; Massuyeau, F.; Gautier, R.; Fateeva, A.; Lebègue, S.; Kim, W. J.; Ledoux, G.; Mesbah, A.; Demessence, A. Tuning the 1D–2D Dimensionality upon Ligand Exchange in Silver Thiolate Coordination Polymers with Photoemission Switching. *J. Mater. Chem. B* **2023**, *11* (18), 3979–3984.
- (12) Okhrimenko, L.; Cibaka Ndaya, C.; Fateeva, A.; Ledoux, G.; Demessence, A. Post-Synthetic Functionalization and Ligand Exchange Reactions in Gold(I) Phenylthiolate-Based Coordination Polymers. *New J. Chem.* **2020**, *44* (41), 17970–17975.
- (13) Sakurada, T.; Cho, Y.; Paritmongkol, W.; Lee, W. S.; Wan, R.; Su, A.; Shcherbakov-Wu, W.; Müller, P.; Kulik, H. J.; Tisdale, W. A. 1D Hybrid Semiconductor Silver 2,6-Difluorophenylselenolate. *J. Am. Chem. Soc.* 2023, 145 (9), 5183–5190.
- (14) Li, Y.; Jiang, X.; Fu, Z.; Huang, Q.; Wang, G.-E.; Deng, W.-H.; Wang, C.; Li, Z.; Yin, W.; Chen, B.; et al. Coordination Assembly of 2D Ordered Organic Metal Chalcogenides with Widely Tunable Electronic Band Gaps. *Nat. Commun.* **2020**, *11* (1), 261.
- (15) Veselska, O.; Dessal, C.; Melizi, S.; Guillou, N.; Podbevšek, D.; Ledoux, G.; Elkaim, E.; Fateeva, A.; Demessence, A. New Lamellar Silver Thiolate Coordination Polymers with Tunable Photoluminescence Energies by Metal Substitution. *Inorg. Chem.* **2019**, *58* (1), 99–105.
- (16) Ke, F.; Zhou, C.; Zheng, M.; Li, H.; Bao, J.; Zhu, C.; Song, Y.; Xu, W. W.; Zhu, M. The Alloying-Induced Electrical Conductivity of Metal—Chalcogenolate Nanowires. *Chem. Commun.* **2021**, *57* (70), 8774—8777.
- (17) Nagaraju Myakala, S.; Rabl, H.; Schubert, J. S.; Batool, S.; Ayala, P.; Apaydin, D. H.; Cherevan, A.; Eder, D. MOCHAs: An Emerging Class of Materials for Photocatalytic H₂ Production. *Small* **2024**, 20 (33), 2400348.
- (18) Schriber, E. A.; Paley, D. W.; Bolotovsky, R.; Rosenberg, D. J.; Sierra, R. G.; Aquila, A.; Mendez, D.; Poitevin, F.; Blaschke, J. P.; Bhowmick, A.; et al. Chemical Crystallography by Serial Femtosecond X-Ray Diffraction. *Nature* **2022**, *601* (7893), 360–365.
- (19) Maserati, L.; Refaely-Abramson, S.; Kastl, C.; Chen, C. T.; Borys, N. J.; Eisler, C. N.; Collins, M. S.; Smidt, T. E.; Barnard, E. S.;

- Strasbourg, M.; et al. Anisotropic 2D Excitons Unveiled in Organic–Inorganic Quantum Wells. *Mater. Horiz.* **2021**, 8 (1), 197–208.
- (20) Rabl, H.; Myakala, S. N.; Rath, J.; Fickl, B.; Schubert, J. S.; Apaydin, D. H.; Eder, D. Microwave-Assisted Synthesis of Metal-Organic Chalcogenolate Assemblies as Electrocatalysts for Syngas Production. *Commun. Chem.* **2023**, *6* (1), 43.
- (21) Lee, W. S.; Cho, Y.; Powers, E. R.; Paritmongkol, W.; Sakurada, T.; Kulik, H. J.; Tisdale, W. A. Light Emission in 2D Silver Phenylchalcogenolates. *ACS Nano* **2022**, *16* (12), 20318–20328.
- (22) Jiang, H.; Cao, L.; Li, Y.; Li, W.; Ye, X.; Deng, W.; Jiang, X.; Wang, G.; Xu, G. Organic "Receptor" Fully Covered Few-Layer Organic—Metal Chalcogenides for High-Performance Chemiresistive Gas Sensing at Room Temperature. *Chem. Commun.* **2020**, *56* (40), 5366–5369.
- (23) Maserati, L.; Prato, M.; Pecorario, S.; Passarella, B.; Perinot, A.; Thomas, A. A.; Melloni, F.; Natali, D.; Caironi, M. Photo-Electrical Properties of 2D Quantum Confined Metal—Organic Chalcogenide Nanocrystal Films. *Nanoscale* **2021**, *13* (1), 233—241.
- (24) Paritmongkol, W.; Lee, W. S.; Shcherbakov-Wu, W.; Ha, S. K.; Sakurada, T.; Oh, S. J.; Tisdale, W. A. Morphological Control of 2D Hybrid Organic–Inorganic Semiconductor AgSePh. *ACS Nano* **2022**, *16* (2), 2054–2065.
- (25) Ye, C.; Li, Z.; Chang, Z.; Wu, S.; Sun, Y.; Xu, W. Dual-Emission 2D Blue Luminescent Organic Silver Chalcogenide for Highly Selective Pb ²⁺ Detection in an Aqueous Medium. *Inorg. Chem.* **2023**, *62* (5), 2334–2341.
- (26) Schriber, E. A.; Popple, D. C.; Yeung, M.; Brady, M. A.; Corlett, S. A.; Hohman, J. N. Mithrene Is a Self-Assembling Robustly Blue Luminescent Metal—Organic Chalcogenolate Assembly for 2D Optoelectronic Applications. ACS Appl. Nano. Mater. 2018, 1 (7), 3498—3508.
- (27) Low, K.-H.; Li, C.-H.; Roy, V. A. L.; Chui, S. S.-Y.; Chan, S. L.-F.; Che, C.-M. Homoleptic Copper(i) Phenylselenolate Polymer as a Single-Source Precursor for Cu2Se Nanocrystals. Structure, Photoluminescence and Application in Field-Effect Transistor. *Chem. Sci.* **2010**, *1* (4), 515.
- (28) Das, A. K.; Biswas, S.; Kayal, A.; Reber, A. C.; Bhandary, S.; Chopra, D.; Mitra, J.; Khanna, S. N.; Mandal, S. Two-Dimensional Silver-Chalcogenolate-Based Cluster-Assembled Material: A *p* -Type Semiconductor. *Nano Lett.* **2023**, 23 (19), 8923–8931.
- (29) Trang, B.; Yeung, M.; Popple, D. C.; Schriber, E. A.; Brady, M. A.; Kuykendall, T. R.; Hohman, J. N. Tarnishing Silver Metal into Mithrene. J. Am. Chem. Soc. 2018, 140 (42), 13892–13903.
- (30) Paritmongkol, W.; Sakurada, T.; Lee, W. S.; Wan, R.; Müller, P.; Tisdale, W. A. Size and Quality Enhancement of 2D Semiconducting Metal—Organic Chalcogenolates by Amine Addition. *J. Am. Chem. Soc.* **2021**, *143* (48), 20256–20263.
- (31) Cuthbert, H. L.; Wallbank, A. I.; Taylor, N. J.; Corrigan, J. F. Synthesis and Structural Characterization of [Cu₂₀Se₄(M₃-SePh)₁₂(PPh₃)₆] and [Ag(SePh)]∞. Z. Anorg. Allg. Chem. **2002**, 628 (11), 2483–2488.
- (32) Powers, E. R.; Paritmongkol, W.; Yost, D. C.; Lee, W. S.; Grossman, J. C.; Tisdale, W. A. Coherent Exciton-Lattice Dynamics in a 2D Metal Organochalcogenolate Semiconductor. *Matter* **2024**, 7 (4), 1612–1630.
- (33) Kastl, C.; Schwartzberg, A. M.; Maserati, L. Picoseconds-Limited Exciton Recombination in Metal—Organic Chalcogenides Hybrid Quantum Wells. *ACS Nano* **2022**, *16* (3), 3715–3722.
- (34) Kastl, C.; Bonfà, P.; Maserati, L. Anharmonic Exciton-Phonon Coupling in Metal-Organic Chalcogenides Hybrid Quantum Wells. *Adv. Opt. Mater.* **2023**, *11* (7), 2202213.
- (35) Yao, K.; Collins, M. S.; Nell, K. M.; Barnard, E. S.; Borys, N. J.; Kuykendall, T.; Hohman, J. N.; Schuck, P. J. Strongly Quantum-Confined Blue-Emitting Excitons in Chemically Configurable Multiquantum Wells. *ACS Nano* **2021**, *15* (3), 4085–4092.
- (36) Paritmongkol, W.; Dahod, N. S.; Stollmann, A.; Mao, N.; Settens, C.; Zheng, S.-L.; Tisdale, W. A. Synthetic Variation and Structural Trends in Layered Two-Dimensional Alkylammonium Lead Halide Perovskites. *Chem. Mater.* **2019**, *31* (15), 5592–5607.

- (37) Lavenn, C.; Okhrimenko, L.; Guillou, N.; Monge, M.; Ledoux, G.; Dujardin, C.; Chiriac, R.; Fateeva, A.; Demessence, A. A Luminescent Double Helical Gold(I)—Thiophenolate Coordination Polymer Obtained by Hydrothermal Synthesis or by Thermal Solid-State Amorphous-to-Crystalline Isomerization. *J. Mater. Chem. C* **2015**, 3 (16), 4115–4125.
- (38) Marsh, R. E. Some Thoughts on Choosing the Correct Space Group. *Acta Crystallogr. B* **1995**, *51* (6), 897–907.
- (39) Holton, J. M.; Frankel, K. A. The Minimum Crystal Size Needed for a Complete Diffraction Data Set. *Acta Crystallogr. D Biol. Crystallogr.* **2010**, *66* (4), 393–408.
- (40) Dahod, N. S.; Paritmongkol, W.; Stollmann, A.; Settens, C.; Zheng, S.-L.; Tisdale, W. A. Melting Transitions of the Organic Subphase in Layered Two-Dimensional Halide Perovskites. *J. Phys. Chem. Lett.* **2019**, *10* (11), 2924–2930.
- (41) Kubelka, P.; Munk, F. An Article on Optics of Paint Layers. Z. Technol. Phys. 1931, 12, 259–274.
- (42) Sheldrick, G. M. SHELXT Integrated Space-Group and Crystal-Structure Determination. *Acta Crystallogr. A Found. Adv.* **2015**, 71 (1), 3–8.
- (43) Sheldrick, G. M. Crystal Structure Refinement with SHELXL. Acta Crystallog.r C Struct. Chem. 2015, 71 (1), 3–8.
- (44) Müller, P. Practical Suggestions for Better Crystal Structures. *Crystallogr. Rev.* **2009**, *15* (1), 57–83.